Supporting Information for

Enhanced energy barriers triggered by magnetic anisotropy modulation via tuning the functional groups on the bridging ligands in Dy_2 single-molecule magnets

Yaru Qin,[a] Yu Jing,[a] Yu Ge,[a] Wei Liu,[a] Yahong Li,*[a] and Yi-Quan Zhang*[b]

[a]College of Chemistry, Chemical Engineering and Materials Science, Soochow University, Suzhou 215123, China

[b]Jiangsu Key Laboratory for NSLSCS, School of Physical Science and Technology, Nanjing Normal University, Nanjing 210023, China

E-mail: liyahong@suda.edu.cn; zhangyiquan@ninu.edu.cn

Supplementary Information Contents

1. Scheme for synthesis of the ligands H_2L_1 and H_2L_2.....2

2. ^1H, ^{13}C NMR spectra of H_2L_1, H_2L_2.....2

3. PXRD patterns of **1** and **2**.....4

4. IR spectra of H_2L_1, H_2L_2, **1** and **2**.....4

5. Selected bond lengths and angles for **1** and **2**.....5

6. Figure for molecular structure of **2**.....6

7. Energy dispersive X- ray spectroscopy (EDS) for **1** and **2**.....7

8. 2D supramolecular framework for **1** generated by hydrogen-bonding interactions.....8

9. Hydrogen-bonding parameters of **1**.....8

10. 1D supramolecular chain of **2** generated by hydrogen-bonding interactions.....8

11. Hydrogen-bonding parameters of **2**.....8

12. MS spectra of complexes **1** and **2**.....9

13. Plots of magnetizations (M) vs dc field (H) for **1** (a) and **2** (b) at 2 K.....10

14. ln τ versus T^{-1} plots for complexes **1** and **2** at high temperature.....10

15. Best fitted parameters for complexes **1** and **2** under 0 Oe dc field.....11

16. Computational details.....12

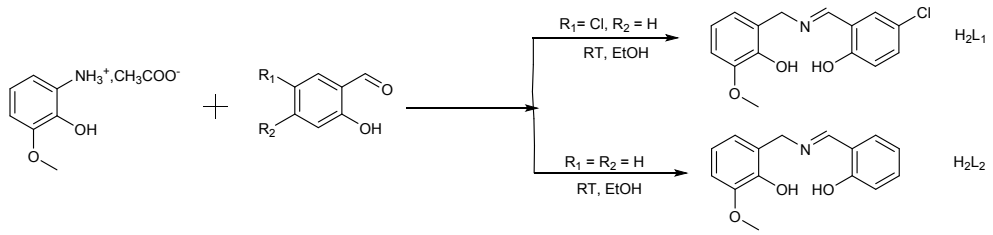

Scheme S1 Synthesis of the ligands H_2L_1 and H_2L_2.

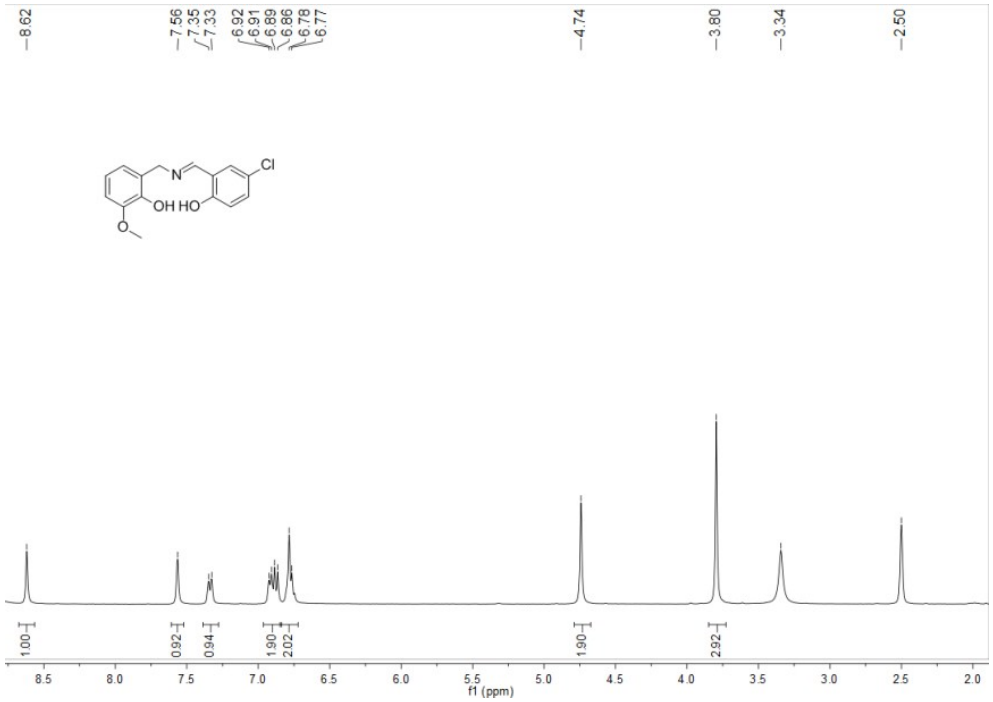

(a)

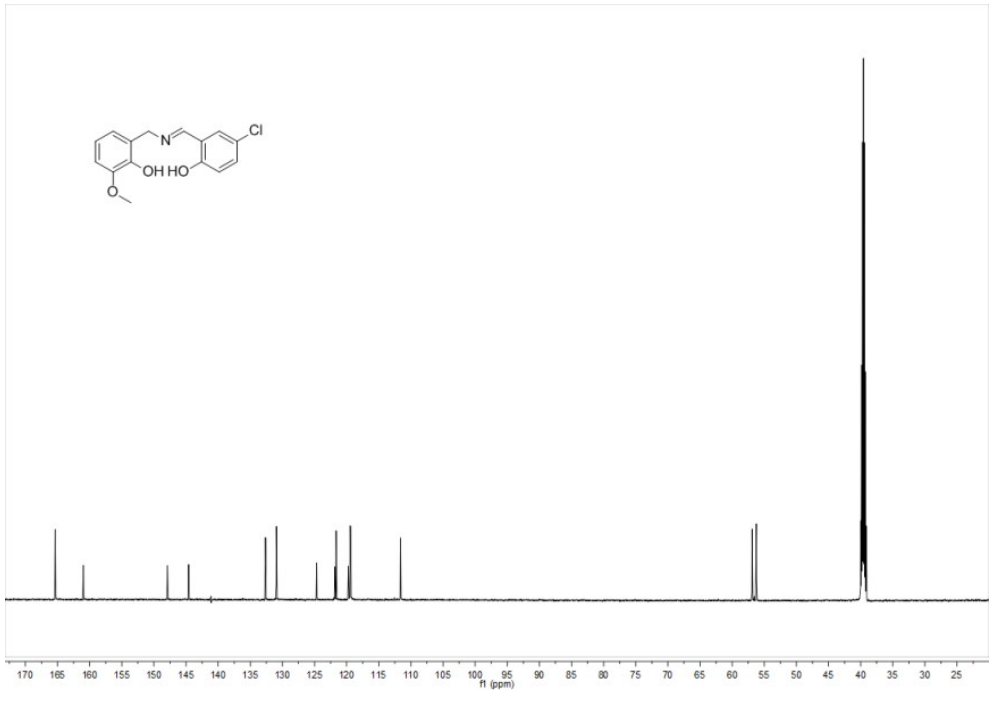

(b)

Fig. S1 The ^{1}H NMR (a) and ^{13}C NMR (b) spectra of H_2L_1.

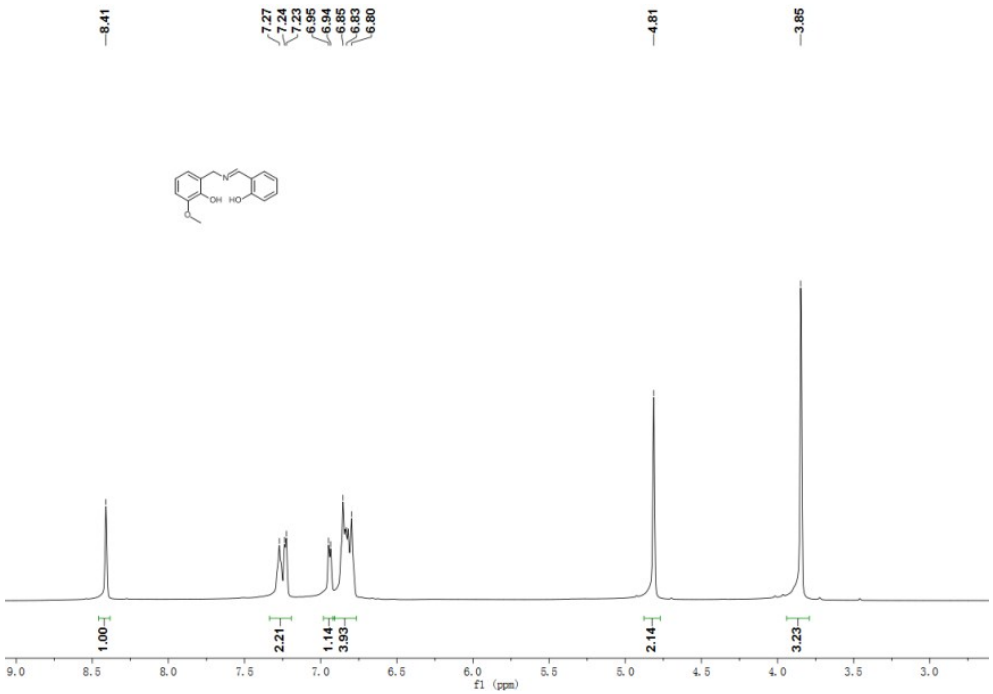

(a)

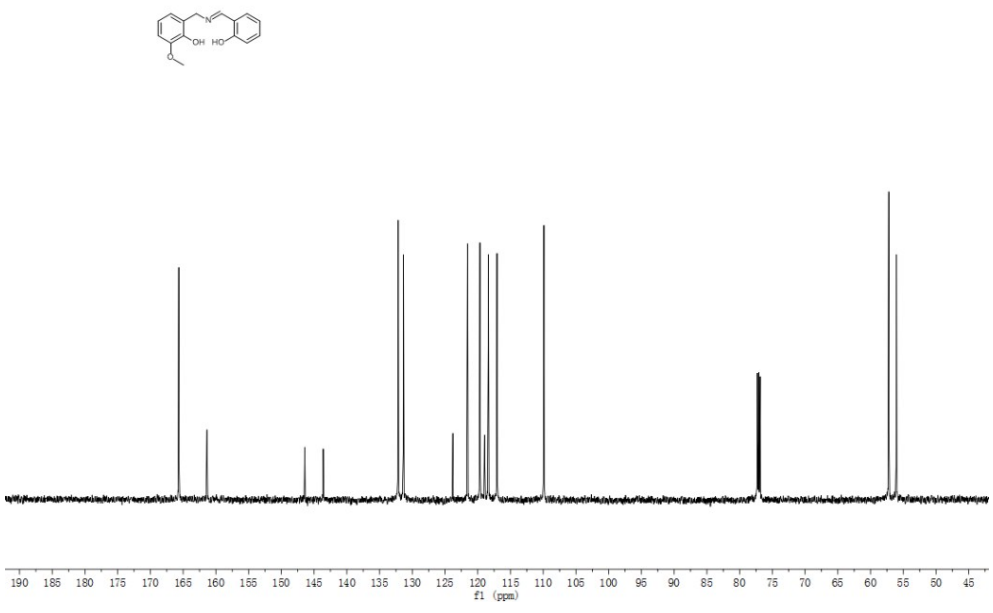

(b)

Fig. S2 The ^{1}H NMR (a) and ^{13}C NMR (b) spectra of H_2L_2.

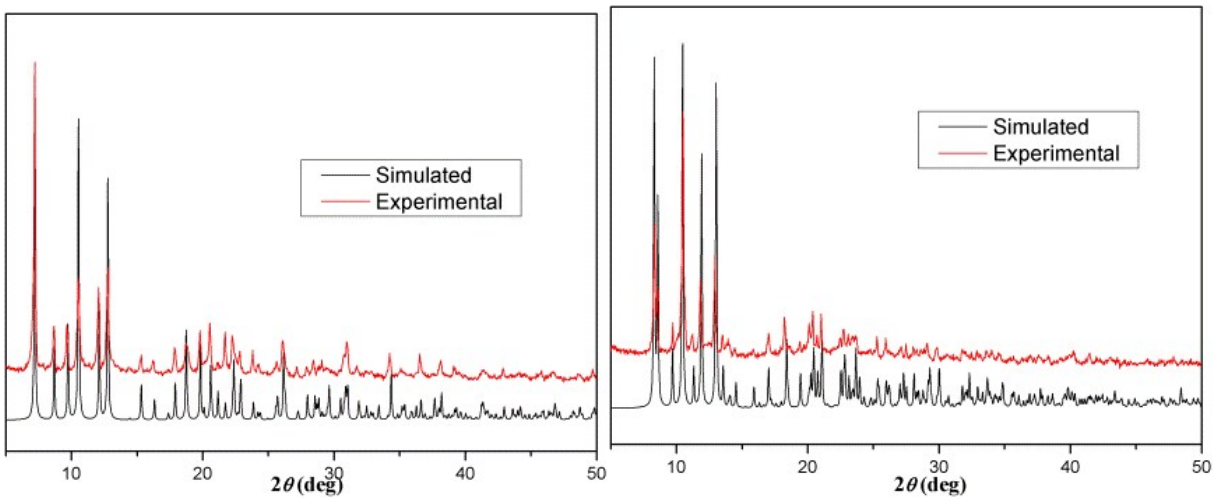

(a) (b)

Fig. S3 PXRD patterns of **1** (a) and **2** (b).

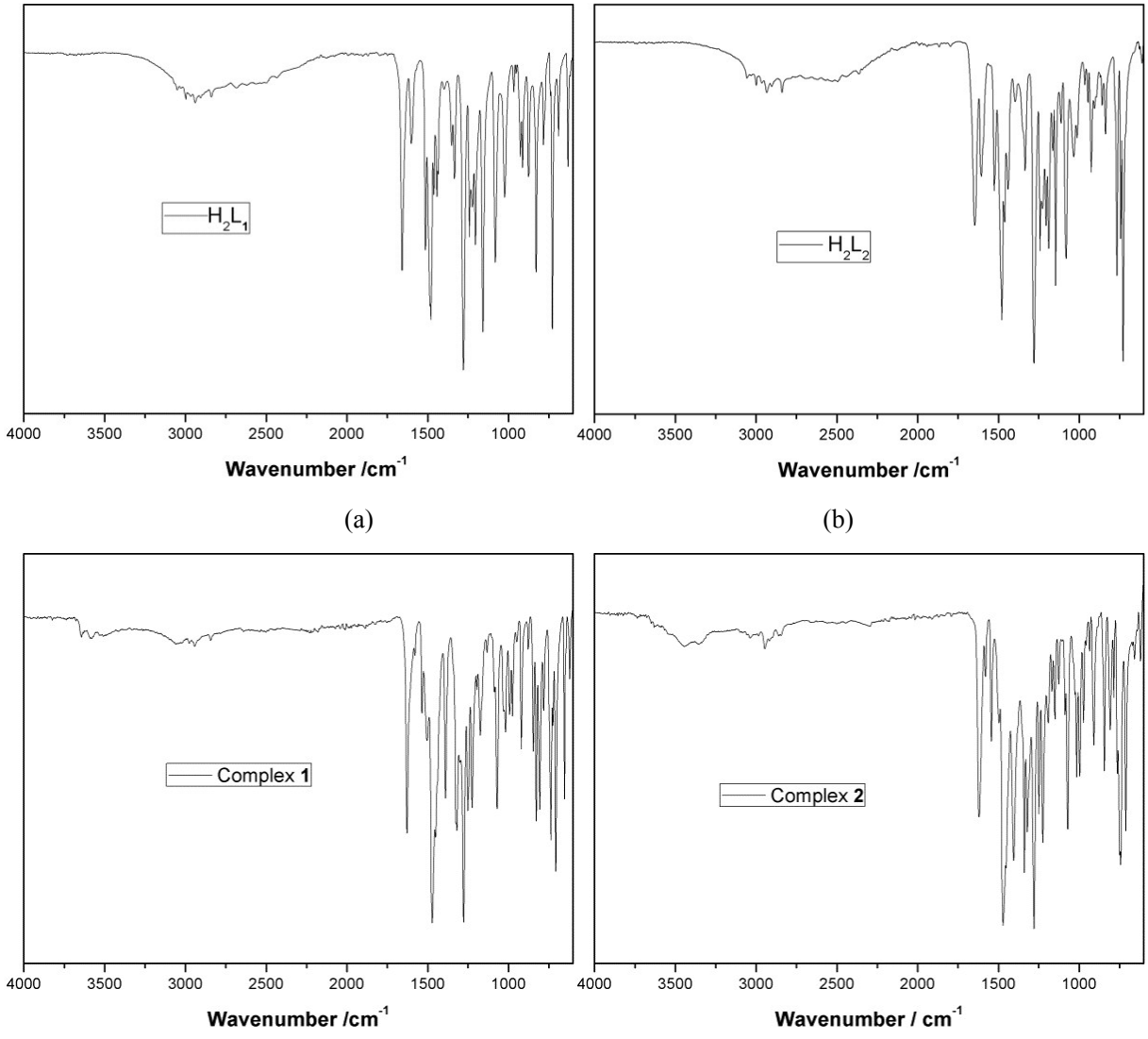

(a) (b)

(c) (d)

Fig. S4 FT-IR spectra of H_2L_1 (a), H_2L_2 (b), **1** (c) and **2** (d).

Table S1. Selected bond lengths (Å) and angle (°) for complexes **1** and **2**.

1			
Dy(1)-O(1)A	2.332(3)	Dy(1)-O(5)	2.436(4)
Dy(1)-O(1)	2.376(3)	Dy(1)-O(2)A	2.512(4)
Dy(1) -O(3)	2.187(4)	Dy(1)-O(7)	2.339(4)
Dy(1)-O(4)	2.502(4)	Dy(1)-N(1)	2.445(5)
O(1)-Dy(1)-O(1)A	66.14(14)	O(1)A-Dy(1)-O(4)	119.24(13)
O(1)-Dy(1)-O(4)	76.33(13)	O(1)A-Dy(1)-O(5)	88.98(14)
O(1)-Dy(1)-O(5)	99.73(15)	O(1)-Dy(1)-O(2)A	130.41(11)
O(1)A-Dy(1)-O(2)A	65.31(12)	O(1)A-Dy(1)-O(7)	78.52(14)
O(1)-Dy(1)-O(7)	105.08(16)	O(1)-Dy(1)-N(1)	77.49(13)
O(1)A-Dy(1)-N(1)	128.67(14)	O(3)-Dy(1)-O(1)A	146.34(13)
O(3)-Dy(1)-O(1)	147.51(12)	O(3)-Dy(1)-O(4)	82.16(15)
O(3)-Dy(1)-O(5)	85.28(14)	O(3)-Dy(1)-O(2)A	81.62(13)
O(3)-Dy(1)-O(7)	87.15(16)	O(3)-Dy(1)-N(1)	76.02(14)
O(4)-Dy(1)-O(2)A	120.50(14)	O(5)-Dy(1)-O(4)	51.81(14)
O(5)-Dy(1)-O(2)A	70.05(15)	O(5)-Dy(1)-N(1)	133.41(15)
O(7)-Dy(1)-O(4)	159.68(14)	O(7)-Dy(1)-O(5)	144.48(16)
O(7)-Dy(1)-O(2)A	74.52(16)	O(7)-Dy(1)-N(1)	77.43(15)
N(1)-Dy(1)-O(4)	83.22(14)	N(1)-Dy(1)-O(2)A	144.73(14)
2			
Dy(1)-O(6)	2.438(5)	Dy(1)-O(4)	2.461(5)
Dy(1)-O(5)	2.465(5)	Dy(1)-O(8)	2.419(5)
Dy(1)-O(3)	2.165(5)	Dy(1)-O(2)	2.336(5)
Dy(1)-O(1)	2.318(5)	Dy(1)-N(1)	2.467(6)
Dy(2)-O(9)	2.155(5)	Dy(2)-O(14)	2.381(5)
Dy(2)-O(10)	2.464(5)	Dy(2)-O(11)	2.534(5)
Dy(2)-O(12)	2.462(5)	Dy(2)-O(2)	2.304(5)
Dy(2)-O(1)	2.337(5)	Dy(2)-N(2)	2.446(6)
O(6)-Dy(1)-O(5)	52.37(16)	O(6)-Dy(1)-O(4)	130.38(17)
O(6)-Dy(1)-N(1)	75.91(18)	O(5)-Dy(1)-N(1)	113.11(18)
O(3)-Dy(1)-O(6)	109.27(18)	O(3)-Dy(1)-O(5)	85.58(17)
O(3)-Dy(1)-O(1)	145.28(17)	O(3)-Dy(1)-O(4)	80.79(17)
O(3)-Dy(1)-O(8)	81.23(18)	O(3)-Dy(1)-O(2)	143.71(16)
O(3)-Dy(1)-N(1)	73.59(19)	O(1)-Dy(1)-O(6)	82.36(16)
O(1)-Dy(1)-O(5)	124.51(16)	O(1)-Dy(1)-O(4)	117.20(17)
O(1)-Dy(1)-O(8)	75.52(16)	O(1)-Dy(1)-O(2)	67.90(16)
O(1)-Dy(1)-N(1)	78.14(18)	O(4)-Dy(1)-O(5)	81.61(17)
O(4)-Dy(1)-N(1)	148.88(18)	O(8)-Dy(1)-O(6)	151.91(17)
O(8)-Dy(1)-O(5)	155.61(17)	O(8)-Dy(1)-O(4)	76.11(18)
O(8)-Dy(1)-N(1)	82.70(18)	O(2)-Dy(1)-O(6)	84.06(17)
O(2)-Dy(1)-O(5)	76.23(17)	O(2)-Dy(1)-O(4)	65.81(16)
O(2)-Dy(1)-O(8)	102.97(17)	O(2)-Dy(1)-N(1)	142.50(17)
O(9)-Dy(2)-O(10)	81.26(17)	O(9)-Dy(2)-O(12)	99.17(17)

O(9)-Dy(2)-O(1)	140.65(16)	O(9)-Dy(2)-O(14)	85.76(18)
O(9)-Dy(2)-O(11)	78.53(17)	O(9)-Dy(2)-O(2)	150.97(17)
O(9)-Dy(2)-N(2)	74.12(18)	O(10)-Dy(2)-O(11)	75.72(16)
O(12)-Dy(2)-O(10)	125.14(16)	O(12)-Dy(2)-O(11)	51.38(16)
O(1)-Dy(2)-O(10)	65.75(15)	O(1)-Dy(2)-O(12)	84.10(16)
O(1)-Dy(2)-O(14)	104.09(17)	O(1)-Dy(2)-O(11)	73.21(16)
O(1)-Dy(2)-N(2)	143.34(17)	O(14)-Dy(2)-O(10)	74.17(16)
O(14)-Dy(2)-O(12)	160.48(17)	O(14)-Dy(2)-O(11)	147.76(17)
O(14)-Dy(2)-N(2)	86.22(18)	O(2)-Dy(2)-O(10)	119.33(16)
O(2)-Dy(2)-O(12)	85.59(17)	O(2)-Dy(2)-O(1)	68.12(16)
O(2)-Dy(2)-O(14)	81.29(18)	O(2)-Dy(2)-O(11)	124.24(16)
O(2)-Dy(2)-N(2)	79.17(18)	N(2)-Dy(2)-O(10)	149.53(17)
N(2)-Dy(2)-O(12)	77.14(18)	N(2)-Dy(2)-O(11)	115.57(17)

Symmetry transformations used to generate equivalent atoms: A: 1-X, 1-Y, +Z

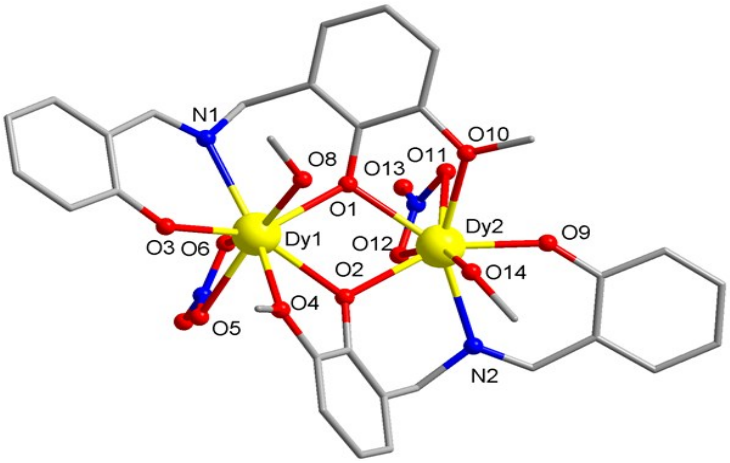

(a)

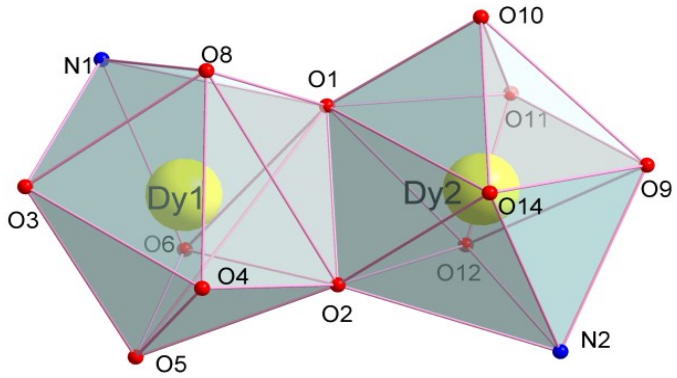

(b)

Fig. S5 (a) Molecular structure of $Dy_2(L_2)_2(NO_3)_2(MeOH)_2$ (**2**). Hydrogen atoms have been omitted for clarity. (b) Coordination polyhedra of Dy^{III} ions in **2**.

Energy dispersive X- ray spectroscopy (EDS)

Energy dispersive X- ray spectroscopies (EDS) for complexes **1** and **2** are shown in Fig S6. Elements C, O, N, Dy and Cl were inclued in complex **1**, while elements C, O, N and Dy Cl were inclued in complex **2**. As Fig. S6 shown, the At% of Dy and Cl is 2:1.9 for **1**, and the At% of Dy and N is 1:2.06 for **2**. The results of EDS are macthed with structures of complexes **1** and **2**.

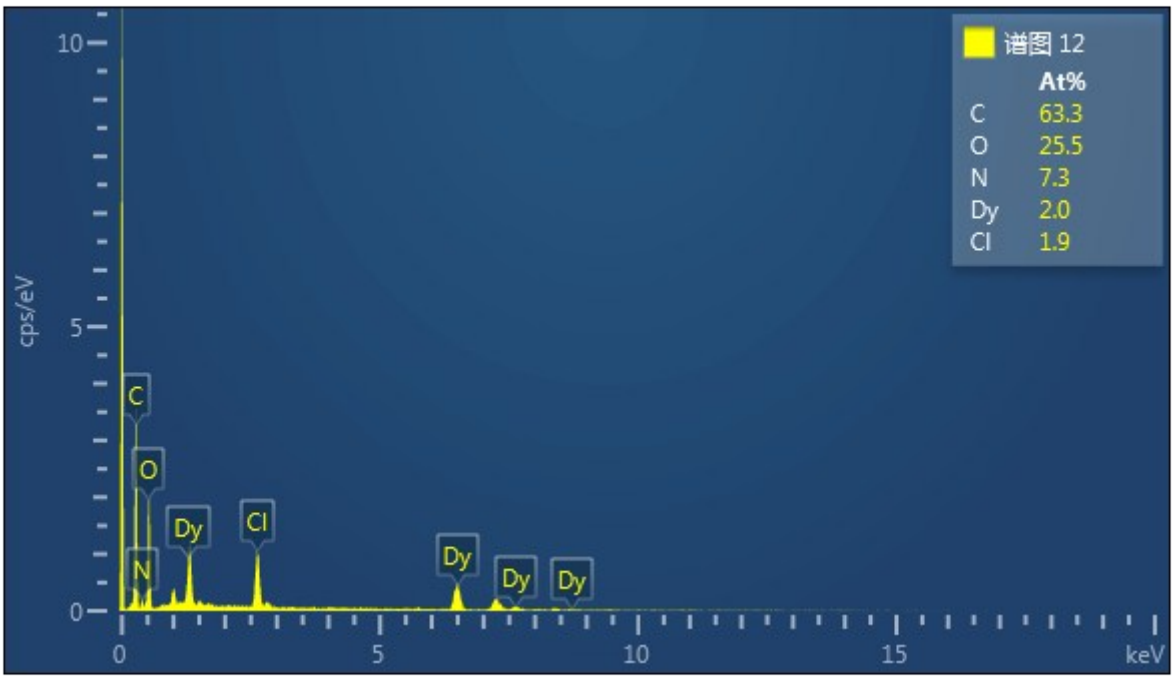

(a)

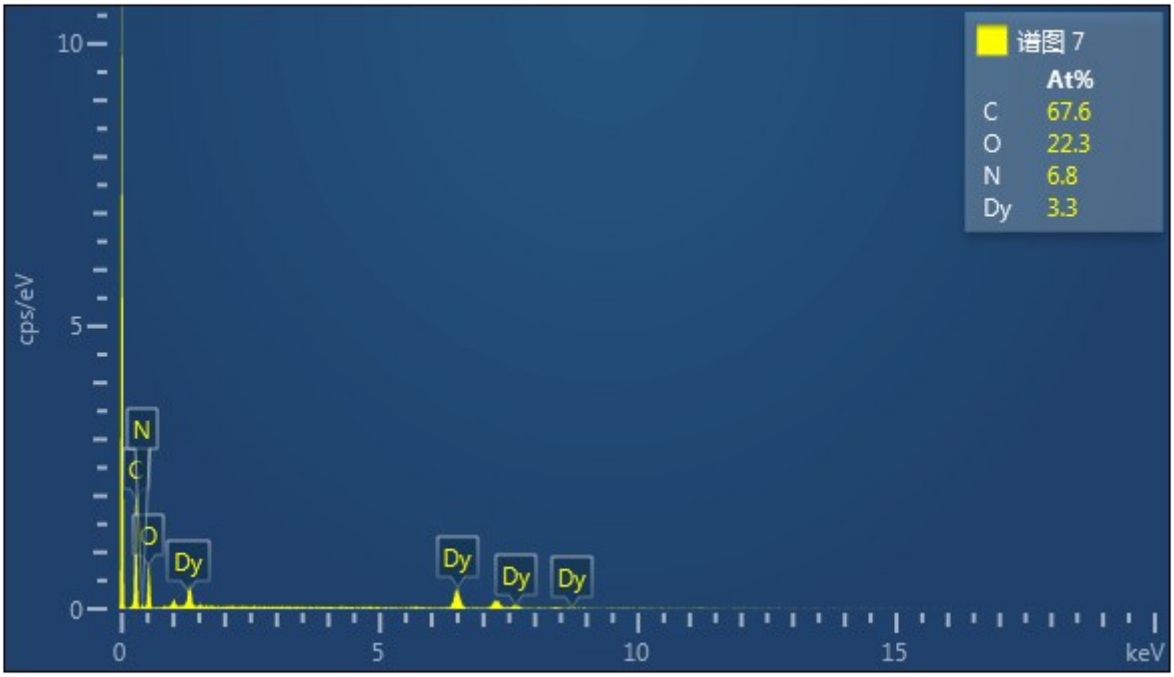

(b)

Fig. S6 (a) Energy dispersive X- ray spectroscopy (EDS) for **1**; (b) Energy dispersive X- ray spectroscopy (EDS) for **2**.

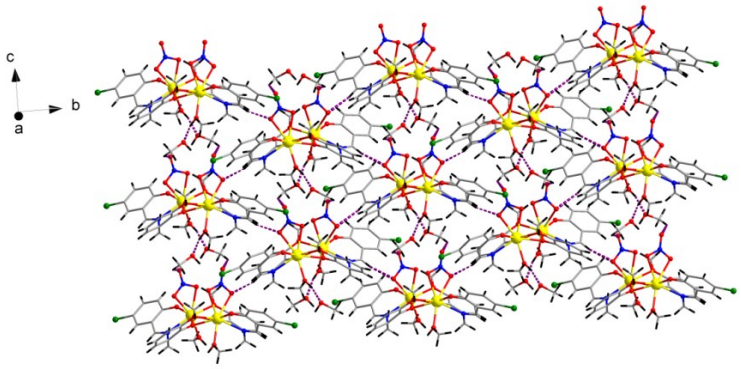

Fig. S7. 2D supramolecular framework of **1** generated by intermolecular hydrogen-bonding interactions.

Table S2. Hydrogen-bonding parameters (Å, deg) of **1**.

D–H···A	*d*(D–H)	*d*(H···A)	D...A	∠D–H···A
O(7)–H(7)···O(8)	0.87(5)	1.71(4)	2.553(8)	165(5)
C(9)–H(9)···O(4)	0.94	2.51	3.390(7)	157
C(17)–H(17A)···O(6)	0.97	2.58	3.247(11)	126

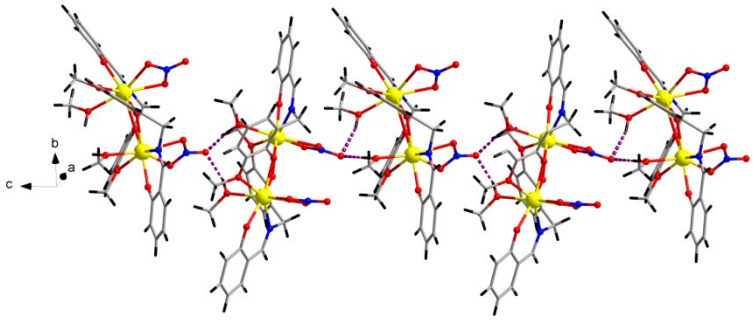

Fig. S8 One-dimensional supramolecular chain of **2** generated by intermolecular hydrogen-bonding interactions.

Table S3. Hydrogen-bonding parameters (Å, deg) of **2**.

D–H···A	*d*(D–H)	*d*(H···A)	*d*(D···A)	∠D–H···A
O(8)–H(8)···O(13)	0.88(2)	1.96(3)	2.810(8)	165(6)
O(14)–H(14)···O(13)	0.88(4)	1.91(5)	2.774(7)	169(4)

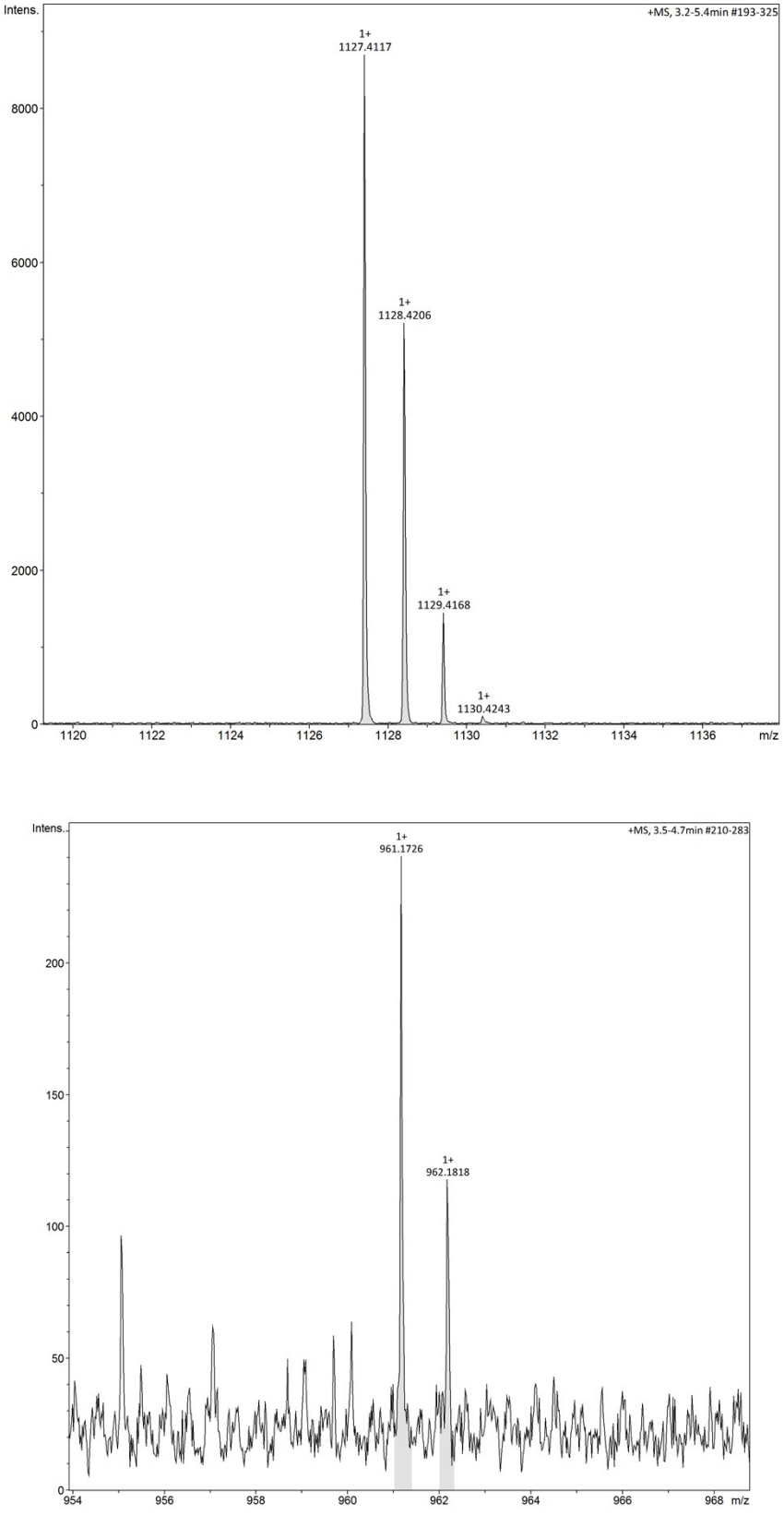

Fig. S9 (a) MS spectrum of complex **1**; (b) MS spectrum of complex **2.**

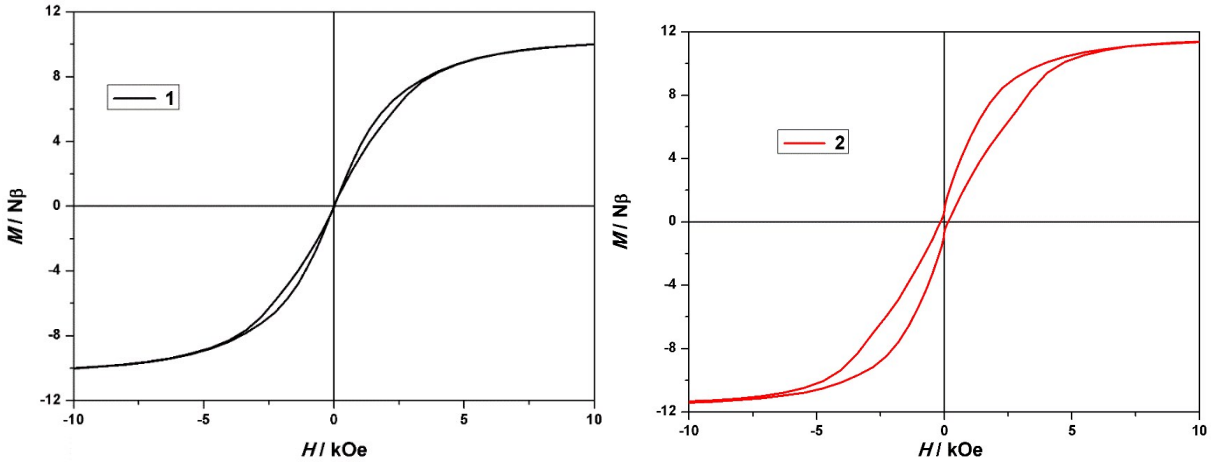

(a) (b)

Fig. S10 Plots of magnetizations (*M*) vs dc field (*H*) for **1** (a) and **2** (b) at 2 K.

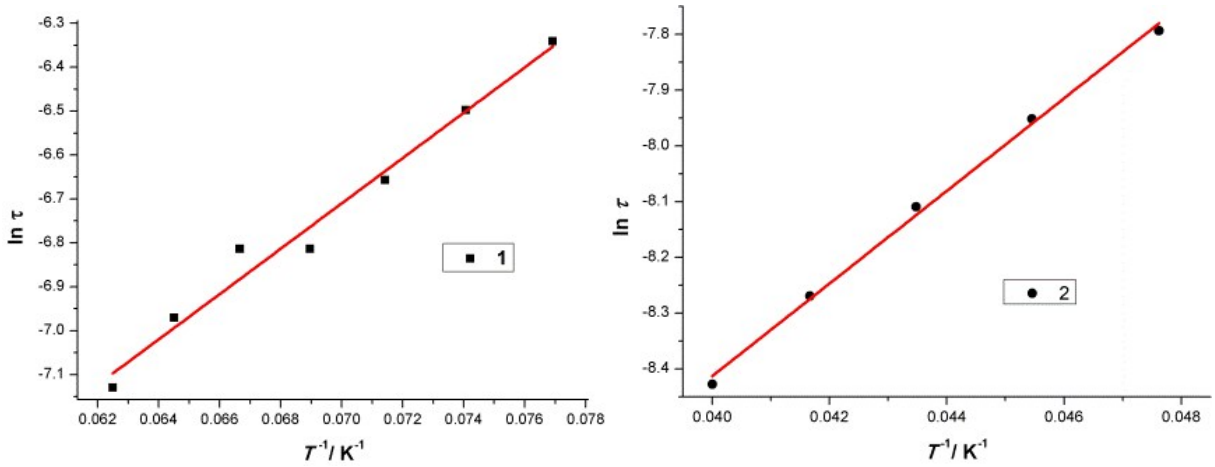

(a) (b)

Fig. S11 ln τ *vs.* T^{-1} plot for **1** (a) and **2** (b) at the high temperature; the solid lines represent the least–squares fits of the experimental data to the Arrhenius law.

Table S4 Best fitted parameters with the extended Debye model for **1** under 0 Oe dc field in the temperature range 6-16 K.

T/K	χ_S	χ_T	τ	α
6	0.381714E-01	0.496999E+01	0.166904E-01	0.129509E+00
6.5	0.276074E-01	0.456940E+01	0.117125E-01	0.129615E+00
7	0.160350E-01	0.424680E+01	0.851252E-02	0.132488E+00
7.5	0.650556E-03	0.398421E+01	0.634482E-02	0.140138E+00
8	0.970757E-03	0.372401E+01	0.480126E-02	0.139155E+00
8.5	0.151818E-02	0.350489E+01	0.371415E-02	0.139520E+00
9	0.982475E-09	0.330764E+01	0.292209E-02	0.141693E+00
9.5	0.148010E-08	0.312868E+01	0.232876E-02	0.141698E+00
10	0.228107E-08	0.296595E+01	0.188103E-02	0.141490E+00
10.5	0.314132E-08	0.281858E+01	0.153595E-02	0.141279E+00
11	0.436442E-08	0.268697E+01	0.126748E-02	0.141416E+00
11.5	0.571573E-08	0.256779E+01	0.105998E-02	0.141539E+00
12	0.558546E-08	0.246068E+01	0.892761E-03	0.141379E+00
12.5	0.743289E-08	0.236652E+01	0.758836E-03	0.141609E+00
13	0.115535E-07	0.227558E+01	0.649164E-03	0.141310E+00
13.5	0.163157E-07	0.219380E+01	0.558541E-03	0.141490E+00
14	0.264759E-07	0.211467E+01	0.483604E-03	0.141485E+00
14.5	0.415237E-07	0.204218E+01	0.421235E-03	0.141850E+00
15	0.658685E-07	0.197201E+01	0.368716E-03	0.142504E+00
15.5	0.101425E-06	0.190778E+01	0.325240E-03	0.144595E+00
16	0.155729E-06	0.184577E+01	0.286886E-03	0.145537E+00

Table S5 Best fitted parameters with the extended Debye model for **2** under 0 Oe dc field in the temperature range 10-25 K.

T/K	χ_S	χ_T	τ	α
10	0.212884E-01	0.292959E+01	0.162653E-01	0.118796E+00
11	0.147100E-01	0.269520E+01	0.103367E-01	0.123166E+00
12	0.591568E-02	0.250973E+01	0.678122E-02	0.127483E+00
13	0.262026E-14	0.232540E+01	0.462619E-02	0.135184E+00
14	0.367578E-14	0.217852E+01	0.326050E-02	0.139836E+00
15	0.540604E-14	0.207410E+01	0.236149E-02	0.146075E+00
16	0.892449E-14	0.194982E+01	0.176483E-02	0.149198E+00
17	0.140218E-13	0.184850E+01	0.132385E-02	0.149312E+00
18	0.245791E-13	0.175163E+01	0.100335E-02	0.146799E+00
19	0.409377E-13	0.165642E+01	0.773132E-03	0.142985E+00
20	0.454971E-13	0.157116E+01	0.602391E-03	0.137239E+00
21	0.675578E-13	0.150338E+01	0.472115E-03	0.129767E+00
22	0.101891E-12	0.142622E+01	0.379273E-03	0.125826E+00
23	0.157391E-12	0.135760E+01	0.304617E-03	0.118268E+00
24	0.234102E-12	0.130380E+01	0.247304E-03	0.111549E+00
25	0.346942E-12	0.125674E+01	0.202816E-03	0.107210E+00

Computational details

Complete-active-space self-consistent field (CASSCF) calculations on lanthanide Dy^{III} fragments of the model structures (see Fig. S11 for the model structures of **1**_***a***, **1**_***b***, **2**_***a*** and **2**_***b***) extracted from the compounds on the basis of single-crystal X-ray determined geometries have been carried out with MOLCAS 8.0 program package (see Fig. S12 for the complete structures of complexes **1** and **2**).[S1] Each dysprosium center was calculated keeping the experimentally determined structure of the corresponding compound while replacing the neighboring Dy^{III} ion by diamagnetic Lu^{III}.

The basis sets for all atoms are atomic natural orbitals from the MOLCAS ANO-RCC library: ANO-RCC-VTZP for Dy^{III} ion; VTZ for close O; VDZ for distant atoms. The calculations employed the second order Douglas-Kroll-Hess Hamiltonian, where scalar relativistic contractions were taken into account in the basis set and the spin-orbit couplings were handled separately in the restricted active space state interaction (RASSI-SO) procedure. For the fragment of individual Dy^{III} ion, active electrons in 7 active spaces include all *f* electrons (CAS(9 in 7)) in the CASSCF calculation. To exclude all the doubts, we calculated all the roots in the active space. We have mixed the maximum number of spin-free state which was possible with our hardware (all from 21 sextets, 128 from 224 quadruplets, 130 from 490 doublets). Single_Aniso[S2] program was used to obtain the ***g*** tensors, energy levels, magnetic axes, *et al.,* based on the above CASSCF/RASSI calculations.

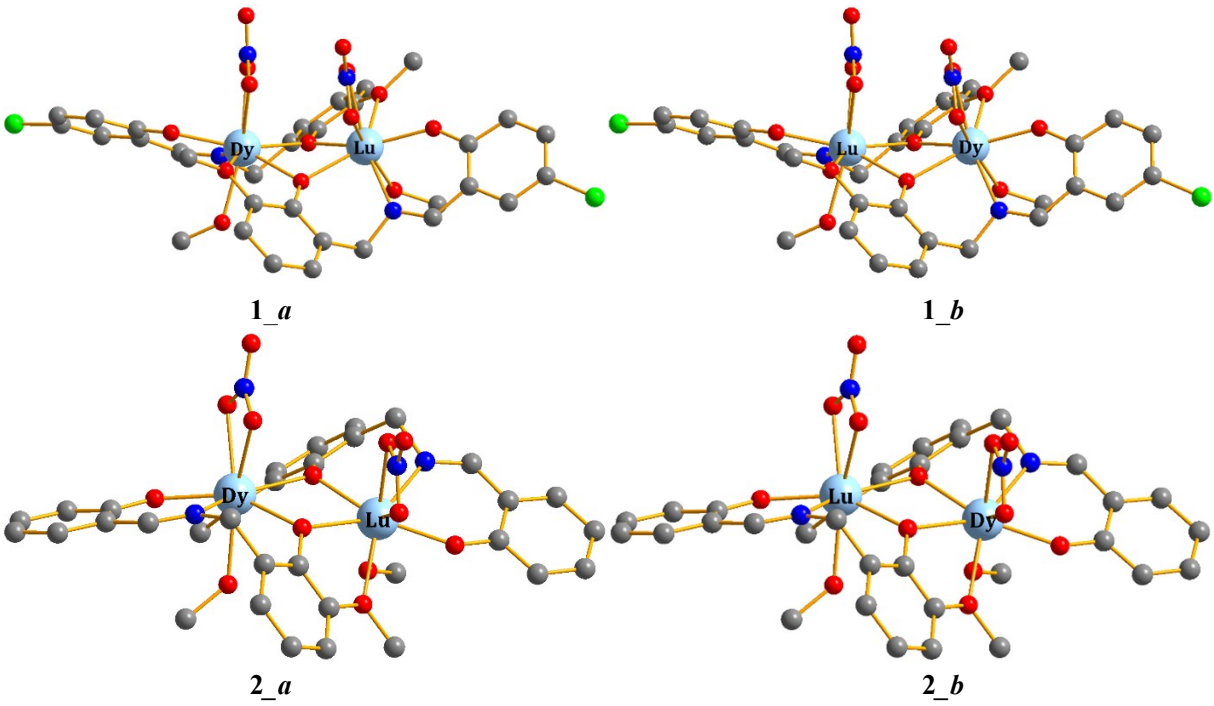

Fig. S12 Calculated model structures of **1_*a***, **1_*b***, **2_*a*** and **2_*b***; H atoms are omitted.

To fit the exchange interaction in the complex, we took two steps to obtain them. Firstly, we calculated each Dy^{III} fragment using CASSCF to obtain the corresponding magnetic properties. Then, the exchange interaction between the magnetic centers is considered within the Lines model,[S3] while the account of the dipole-dipole magnetic coupling is treated exactly. The Lines model is effective and has been successfully used widely in the research field of f-element single-molecule magnets.[S4]

The exchange Ising Hamiltonian is:

$$\hat{H}_{exch} = -J_{total}\,\hat{S}_{Dy1}\,\hat{S}_{Dy2} \qquad \text{(S1)}$$

The J_{total} is the parameter of the total magnetic interaction ($J_{total} = J_{diploar} + J_{exchange}$) between magnetic center ions. The $\hat{S}_{Dy}$ = ±1/2 are the ground pseudospin on the Dy^{III} sites. The dipolar magnetic coupling can be calculated exactly, while the exchange coupling constants were fitted through comparison of the computed and measured magnetic susceptibilities using the POLY_ANISO program.[S2]

Table S6 Calculated energy levels (cm^{-1}), ***g*** (g_x, g_y, g_z) tensors and m_J values of the lowest Kramers doublets (KDs) of individual Dy^{III} fragments of **1_*a***, **1_*b***, **2_*a*** and **2_*b***.

KDs	**1_*a***			**1_*b***		
	E/cm^{-1}	***g***	m_J	E/cm^{-1}	***g***	m_J
1	0.0	0.002 0.004 19.686	±15/2	0.0	0.003 0.005 19.723	±15/2
2	234.0	0.059 0.075 16.860	±13/2	229.8	0.053 0.070 16.935	±13/2
3	383.9	1.254 1.438 13.075	±11/2	385.0	1.039 1.223 13.223	±11/2
4	460.1	4.838 5.922 10.123	±7/2	458.3	4.621 5.942 10.960	±5/2
5	508.5	0.253 2.718 13.487	±1/2	506.7	0.280 2.283 13.775	±1/2
6	569.6	0.837 1.906 14.344	±5/2	570.0	1.053 1.997 14.511	±7/2
7	599.3	0.968 2.343 15.957	±3/2	597.9	1.126 2.463 15.696	±3/2

8	641.8	0.233 0.546 18.824	±9/2	636.9	0.286 0.775 18.698	±9/2
KDs	**2_*a***			**2_*b***		
	E/cm^{-1}	***g***	m_J	E/cm^{-1}	***g***	m_J
1	0.0	0.001 0.003 19.696	±15/2	0.0	0.003 0.004 19.732	±15/2
2	229.8	0.023 0.023 16.857	±13/2	267.2	0.086 0.119 16.644	±13/2
3	400.4	0.268 0.363 13.778	±11/2	454.0	0.723 0.874 13.480	±11/2
4	511.2	4.486 5.475 9.195	±9/2	582.5	3.967 4.898 9.254	±9/2
5	584.8	0.929 4.882 10.066	±5/2	672.6	3.356 3.918 11.647	±5/2
6	627.6	1.562 2.379 16.058	±1/2	752.3	10.097 8.141 0.100	±1/2
7	662.6	0.170 0.568 17.680	±3/2	766.1	11.446 6.750 0.529	±3/2
8	772.1	0.016 0.022 19.608	±7/2	832.5	0.072 0.157 19.355	±7/2

Table S7 Exchange energies (cm^{-1}) and main values of the g_z for the lowest two exchange doublets of **1** and **2**.

	1		**2**	
	E/cm^{-1}	g_z	E/cm^{-1}	g_z
1	0.0	38.333	0.0	39.138
2	3.0	9.143	2.6	4.771

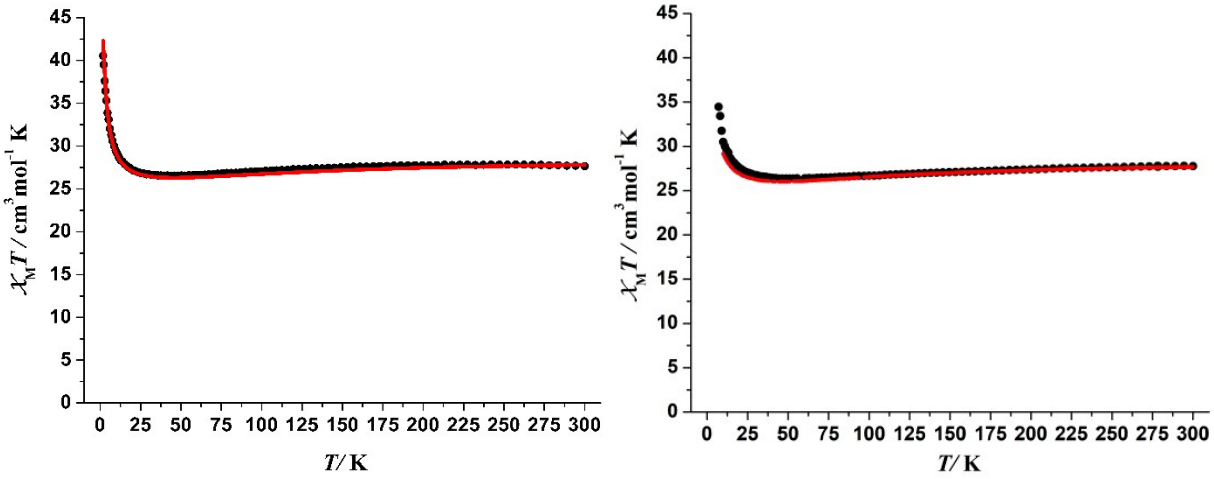

(a) (b)

Fig. S13 Calculated (red solid line) and experimental (circle dot) data of magnetic susceptibilities of complexes **1**(a) and **2**(b). The intermolecular interactions zJ' of **1** and **2** were fitted to 0.00 and −0.02 cm^{-1}, respectively.

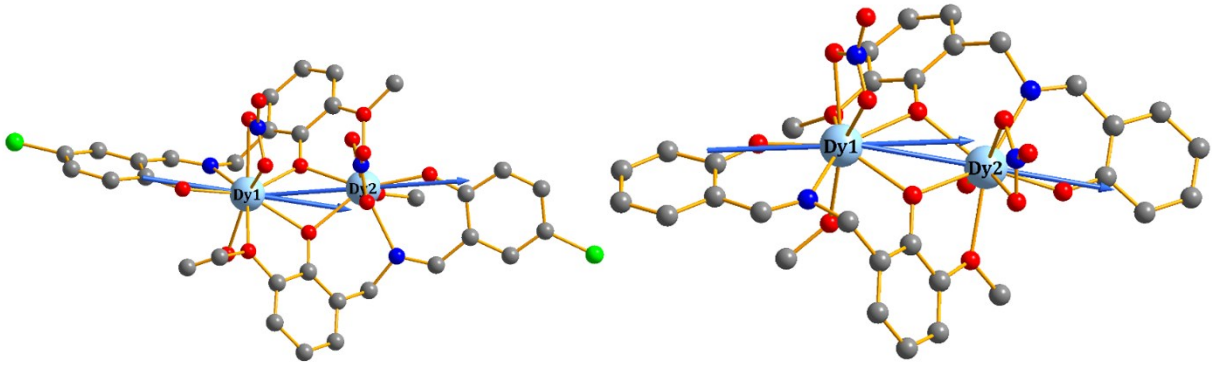

(a) (b)

Fig. S14 Calculated orientations of the local main magnetic axes of the ground Kramers doublet on Dy^{III} ions of complexes **1** (a) and **2** (b).

Table S8. Included angle (θ) between the local main magnetic axis of the ground Kramers doublet on Dy_1 (θ_1) or Dy_2 (θ_2) and the vector connecting the two Dy^{III} ions for complexes **1** and **2**.

	1	**2**
θ_1	14.47°	11.08°
θ_2	14.84°	4.34°

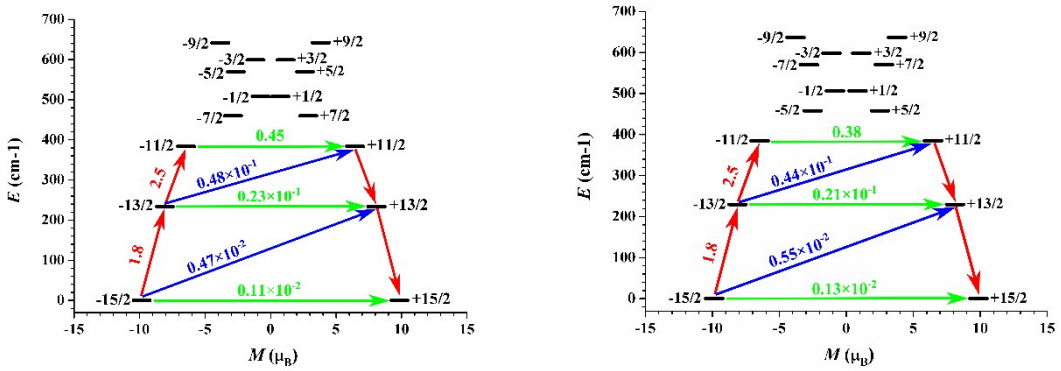

1_*a* **1_*b***

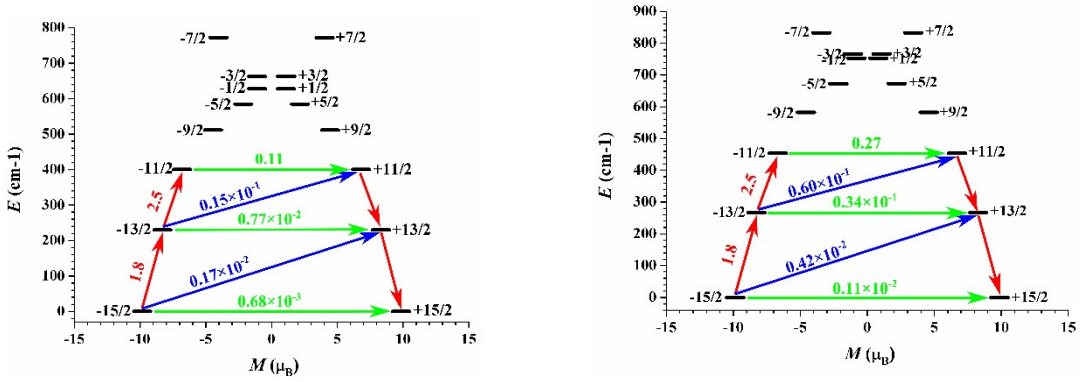

2_*a* **2_*b***

Fig. S15 The magnetization blocking barriers in **1_*a***, **1_*b***, **2_*a*** and **2_*b***. The thick black lines represent the Kramers doublets as a function of their magnetic moment along the magnetic axis. The green lines correspond to diagonal quantum tunneling of magnetization (QTM); the blue line represent off-diagonal relaxation process. The numbers at each arrow stand for the mean absolute value of the corresponding matrix element of transition magnetic moment.

References:

S1 (a) Aquilante, F.; De Vico, L.; Ferré, N.; Ghigo, G.; Malmqvist, P.-Å.; Neogrády, P.; Pedersen, T. B.; Pitonak, M.; Reiher, M.; Roos, B. O.; Serrano-Andrés, L.; Urban, M.; Veryazov, V.; Lindh, R. *J. Comput. Chem*., **2010**, *31*, 224. (b) Veryazov, V.; Widmark, P. -O.; Serrano-Andres, L.; Lindh, R.; Roos, B. O. *Int. J. Quantum Chem*., **2004**, *100*, 626. (c) Karlström, G.; Lindh, R.; Malmqvist, P. -Å.; Roos, B. O.; Ryde, U.; Veryazov, V.; Widmark, P. -O.; Cossi, M.; Schimmelpfennig, B.; Neogr´ady, P.; Seijo, L. *Comput. Mater. Sci*., **2003**, *28*, 222.

S2 (a) Chibotaru, L. F.; Ungur, L.; Soncini, A. *Angew. Chem. Int. Ed.*, **2008**, *47*, 4126. (b) Ungur, L.; Van den Heuvel, W.; Chibotaru, L. F. *New J. Chem.*, **2009**, *33*, 1224. (c) Chibotaru, L. F.; Ungur, L.; Aronica, C.; Elmoll, H.; Pilet, G.; Luneau, D. *J. Am. Chem. Soc.*, **2008**, *130*, 12445.

S3 Lines, M. E. *J. Chem. Phys*. **1971**, *55*, 2977.

S4 (a) Mondal, K. C.; Sundt, A.; Lan, Y. H.; Kostakis, G. E.; Waldmann, O.; Ungur, L.; Chibotaru, L. F.; Anson, C. E.; Powell, A. K. *Angew. Chem. Int. Ed*. **2012**, *51*, 7550. (b) Langley, S. K.; Wielechowski, D. P.; Vieru, V.; Chilton, N. F.; Moubaraki, B.; Abrahams, B. F.; Chibotaru, L. F.; Murray, K. S. *Angew. Chem. Int. Ed*. **2013**,